Expanded View Figures

Figure EV1. The overall structure of the RshSTT182/200 RBD bound to hACE2.

A Structure-based sequence alignment of the SARS-CoV-2 and RshSTT182/200 RBDs. The secondary structure elements were defined based on an ESPript (Robert & Gouet, 2014) algorithm and are labeled based on the SARS-CoV-2 RBD/hACE2 complex structure (PDB: 6LZG). Coils indicate α helices, and black arrows indicate β strands. Conserved residues are highlighted in red and residues in blue boxes are highly (80%) conserved. Residues of the SARS-CoV-2 RBD and RshSTT182/200 RBD that contact hACE2 through van der Waals interactions are marked with red regular triangles and blue inverted triangles, respectively. The sequence alignment was generated with SnapGene and ESPript.

B The secondary structural elements of the RshSTT182/200 RBD are defined.

C Flow cytometry characterization of the RshSTT182/200 or SARS-CoV-2 RBDs binding to hACE2. The SARS-CoV-2 NTD was used as a negative control. The frequency of RBD-positive cells in the hACE2-eGFP-positive cells is labeled in the upper right corner.

D Gel filtration profiles of hACE2 (blue), the RshSTT182/200 RBD (saffron yellow), and the RshSTT182/200 RBD/hACE2 complex (red) were analyzed and are displayed. The separation profiles of each of the pooled samples on SDS–PAGE are shown.

E The comparison of the overall structure of the RshSTT182/200 RBD/hACE2 complex compared to the SARS-CoV-2 RBD/hACE2 complex structure.

F Structural alignment of hACE2 in the RBD/ACE2 complexes. hACE2 in complex with the RshSTT182/200 RBD and SARS-CoV-2 RBD (PDB: 6LZG) is shown in salmon and green, respectively. The black lines show the difference between the open and closed states of the α4-helix.

G The α2-helix and α4-helix of hACE2 in the RshSTT182/200 RBD/hACE2 complex (closed state) and SARS-CoV-2 RBD/hACE2 complex (open state) are shown.

H Structural alignment of free hACE2 and hACE2 in the RBD/ACE2 complex. Free hACE2 (PDB: 1R42) is shown in teal.

I–L Comparison of the overall structure of the RshSTT182/200 RBD/hACE2 complex with the SARS-CoV RBD/hACE2 (PDB: 2AJF), GX/P2V/2017 RBD/hACE2 (PDB: 7DDP), GD/1/2019 RBD/hACE2 (PDB: 7DDO), or RaTG13 RBD/hACE2 (PDB: 7DRV) complex.

Source data are available online for this figure.

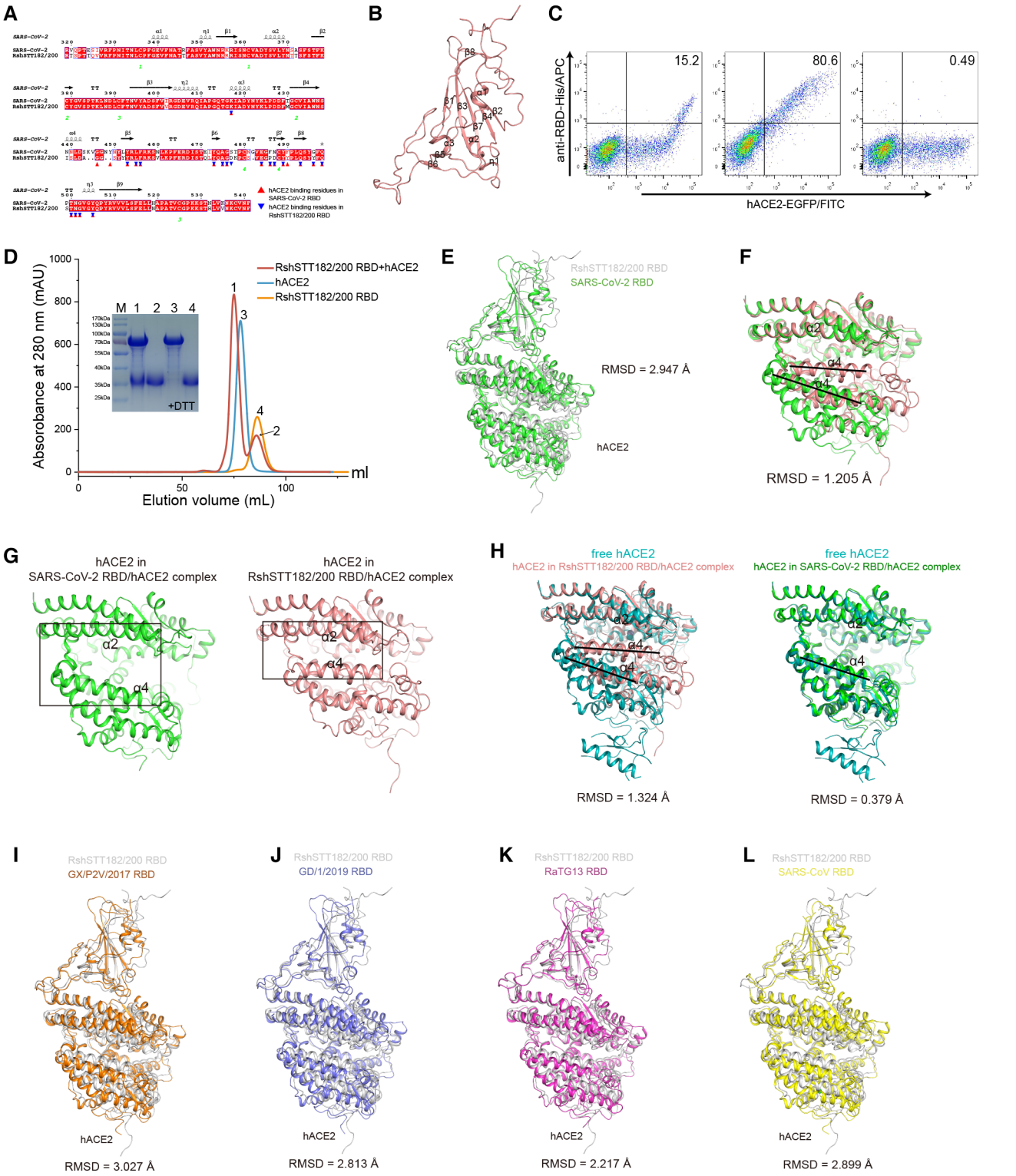

Figure EV1.

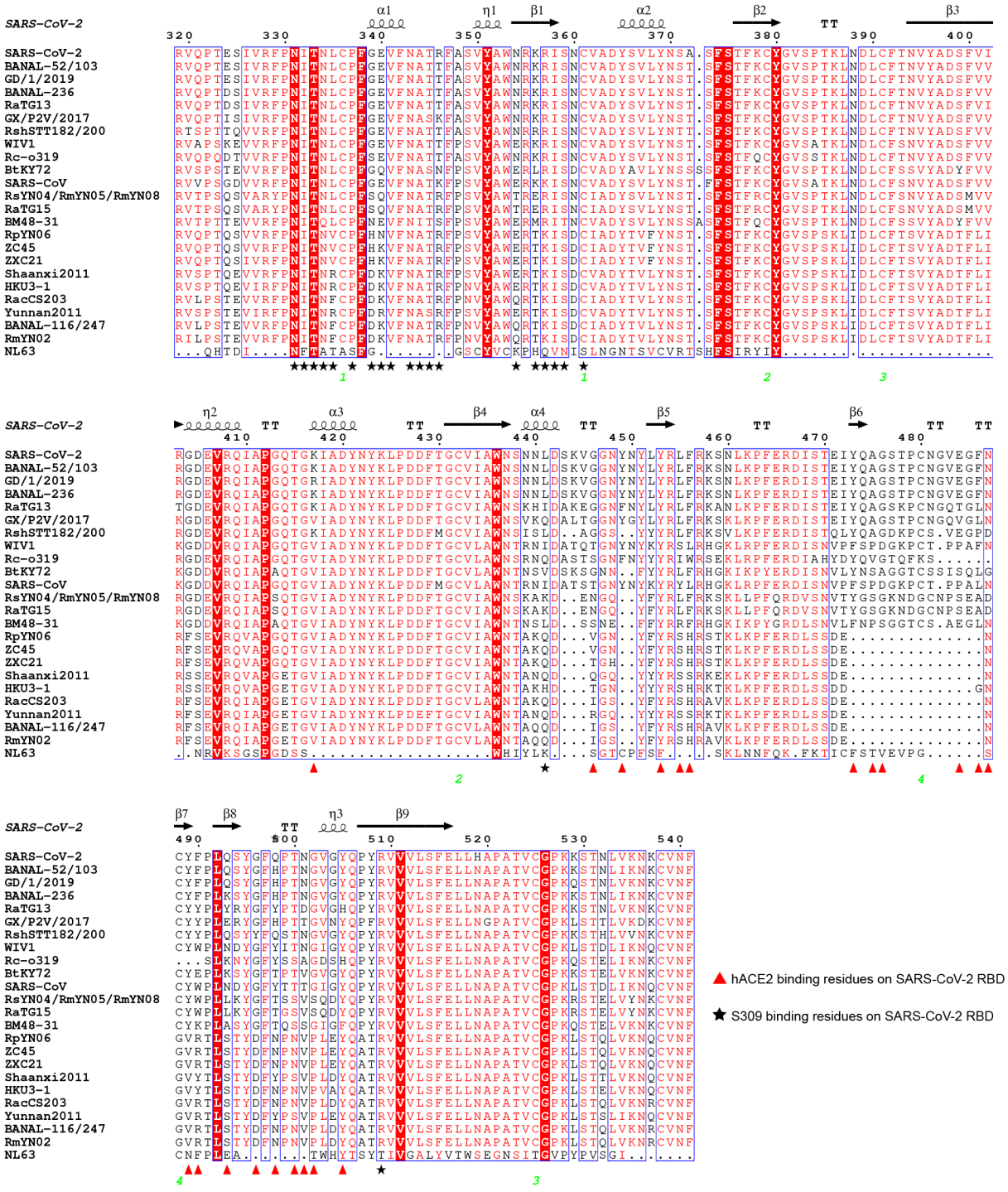

Figure EV2. Structure-based sequence alignment of the RBD of CoVs.

The figure label is as described in Fig EV1A.

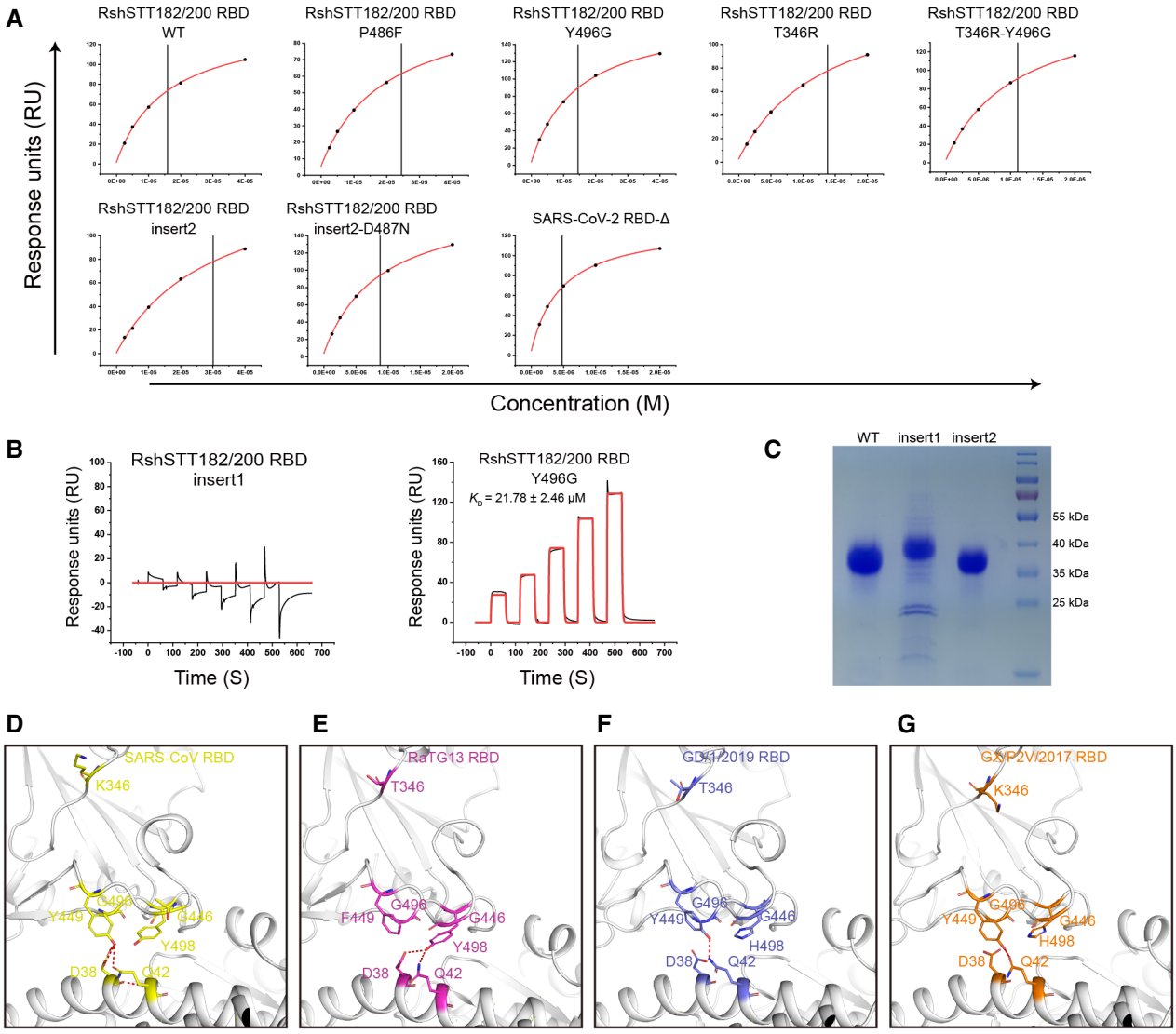

Figure EV3. SPR characterization of hACE2 binding to the RshSTT182/200 RBD and its mutants.

hACE2 with hFc tag was captured by a protein A chip and sequentially tested for the binding with serially diluted RshSTT182/200 RBD or mutants by SPR.

A The steady-state fitting curve is shown when the K_D was calculated by the steady-state model.

B SPR analysis of hACE2 binding to the RshSTT182/200 RBD insert1 and Y496G. The raw and fitted curves are displayed as black and red lines, respectively.

C SDS–PAGE showing the difference in molecular weight among RshSTT182/200 RBD-WT, RBD-insert1, and RBD-insert2.

D–G The H-bond interactions of the β4β5 loop region of the SARS-CoV RBD, RaTG13 RBD, GD/1/2019 RBD, and GX/P2V/2017 RBD are shown.

Source data are available online for this figure.

Figure EV4. SPR characterization of ACE2s binding to the RshSTT182/200 RBD, as well as the key residue contacts between hACE2 and the RshSTT182/200 or SARS-CoV-2 RBDs.

A Representative example of sensorgrams and binding kinetics model fitting of ACE2 (mFc-tagged ACE2) binding to the RshSTT182/200 RBD by SPR analysis. ACE2s in supernatants were captured by anti-mIgG Fc antibodies immobilized on the CM5 chip, and binding to serially diluted RshSTT182/200 RBD was sequentially tested. The raw and fitted curves are displayed as black and red lines, respectively.

B The saturation curve fitted to the response (RU) at equilibrium was plotted against the protein concentration when K_D was estimated by steady-state fitting. The binding affinity with rapid dissociation and association rates (K_d and K_a) makes the kinetic fitting inaccurate.

C Residues in hACE2 that form contacts with the RBD are listed. The numbers with asterisks indicate that the key residue only interacts with the SARS-CoV-2 RBD. The conserved residues among the 39 ACE2 orthologs are shown as black letters, and the residue substitutions in the ACE2 of 38 species relative to hACE2 are shown as red letters. The gray background represents the binding of the RshSTT182/200 RBD to the ACE2 of this species.

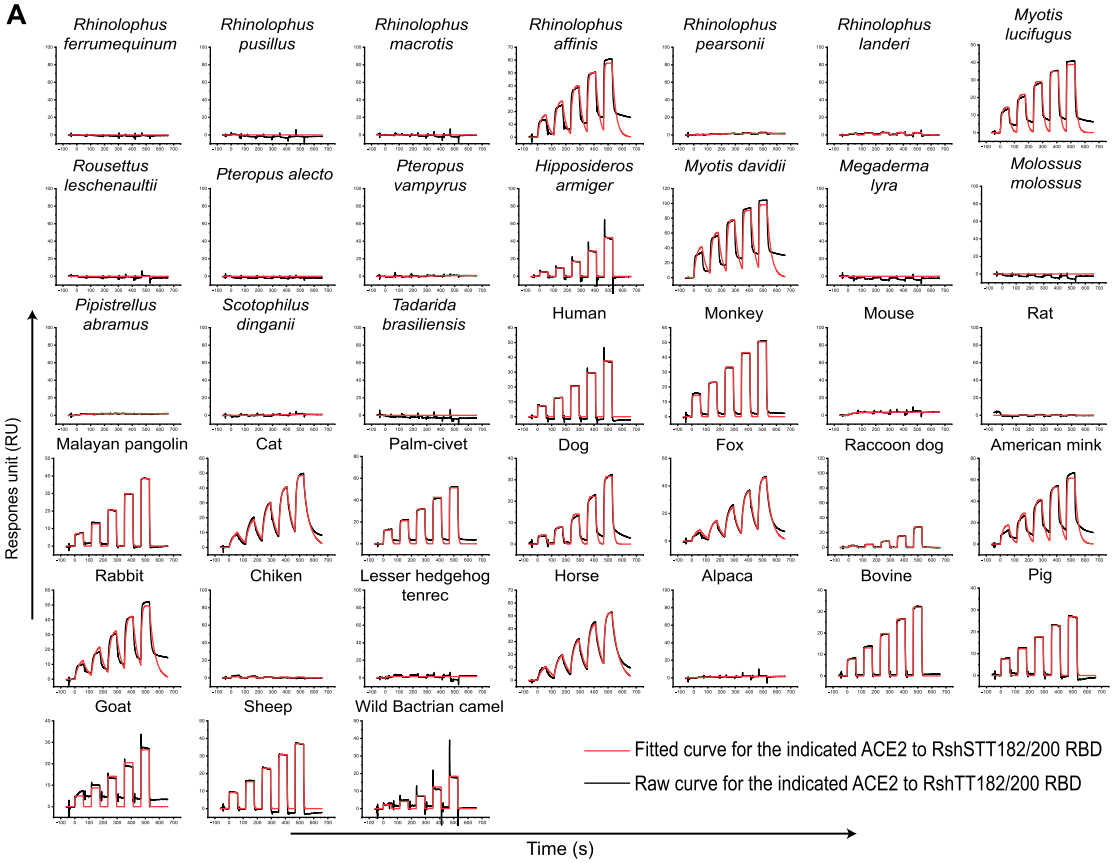

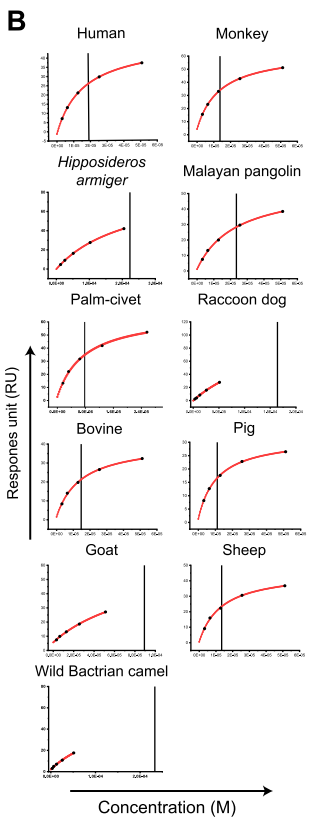

C

	19	24	27	28	30	31	34	35	37	38	41	42	45	79	82*	83	330	353	354	355	357	393	Substitutions
Human	S	Q	T	F	D	K	H	E	E	D	Y	Q	L	L	M	Y	N	K	G	D	R	R	
Rhinolophus shameli	S	R	A	F	D	K	P	E	E	E	H	Q	L	L	N	F	N	K	N	D	R	R	8
Rhinolophus ferrumequinum	S	L	K	F	D	D	S	E	E	N	H	Q	L	L	N	F	N	K	G	D	R	R	8
Rhinolophus pusillus	S	K	K	F	N	D	S	E	E	D	Y	Q	L	I	N	Y	N	K	G	D	R	R	6
Rhinolophus macrotis	S	E	K	F	D	K	S	K	E	D	Y	E	L	L	N	Y	K	K	G	D	R	R	7
Rhinolophus affinis	S	R	I	F	D	N	R	E	E	E	Y	Q	L	L	N	Y	N	K	G	D	R	R	6
Rhinolophus pearsonii	S	R	T	F	D	K	H	E	E	D	H	E	L	L	D	Y	N	K	D	D	R	R	5
Rhinolophus landeri	S	L	T	F	D	D	S	A	E	N	Y	Q	L	H	N	F	N	K	G	D	R	R	8
Myotis lucifugus	S	K	I	F	E	N	S	K	E	D	H	E	L	L	T	Y	N	K	G	D	R	R	9
Rousettus leschenaultii	S	L	T	F	E	K	T	E	E	D	Y	Q	L	L	T	Y	K	K	G	D	R	R	5
Pteropus alecto	S	L	T	F	E	K	T	E	E	D	Y	Q	L	L	A	Y	K	K	G	D	R	K	6
Pteropus vampyrus	S	L	T	F	E	K	T	E	E	D	Y	Q	L	L	A	Y	K	K	G	D	R	K	6
Hipposideros armiger	S	L	E	F	D	K	T	E	E	D	H	L	L	R	D	Y	N	K	G	D	R	R	7
Myotis davidii	S	K	I	F	D	N	S	K	E	D	H	E	L	L	T	Y	N	K	G	D	R	R	8
Megaderma lyra	S	Q	T	F	E	K	L	E	E	E	Y	Q	L	L	H	F	N	K	N	D	R	R	6
Molossus molossus	S	K	I	F	D	N	I	R	E	E	H	Q	L	Q	M	Y	N	N	N	D	R	R	10
Pipistrellus abramus	Y	E	R	F	V	K	H	E	E	N	H	E	L	I	G	F	D	K	N	D	R	R	11
Scotophilus dinganii	S	K	I	F	E	S	S	K	E	D	Y	E	I	L	T	Y	N	K	G	D	R	R	8
Tadarida brasiliensis	S	E	I	F	Q	R	T	E	E	E	H	Q	L	H	R	Y	N	K	G	D	R	R	9
Monkey	S	Q	T	F	D	K	H	E	E	D	Y	Q	L	L	M	Y	N	K	G	D	R	R	0
Mouse	S	N	T	F	N	N	Q	E	E	D	Y	Q	L	T	S	F	N	H	G	D	R	R	8
Rat	S	K	S	F	N	K	Q	E	E	D	Y	Q	L	I	N	F	N	H	G	D	R	R	8
Malayan pangolin	S	E	T	F	E	K	S	E	E	E	Y	Q	L	I	N	Y	N	K	H	D	R	R	7
Cat	S	L	T	F	E	K	H	E	E	E	Y	Q	L	L	T	Y	N	K	G	D	R	R	4
Palm-civet	S	L	T	F	E	T	Y	E	Q	E	Y	Q	V	L	T	Y	N	K	G	D	R	R	8
Dog	S	L	T	F	E	K	Y	E	E	E	Y	Q	L	L	T	Y	N	K	G	D	R	R	5
Fox	S	L	T	F	E	K	Y	E	E	E	Y	Q	L	L	T	Y	N	K	G	D	R	R	5
Raccoon dog	S	L	T	F	E	K	Y	E	E	E	Y	Q	L	L	T	Y	N	R	G	D	R	R	6
American mink	S	L	T	F	E	K	Y	E	E	E	Y	Q	L	H	T	Y	N	K	H	D	R	R	7
Rabbit	S	L	T	F	E	K	Q	E	E	D	Y	Q	L	L	T	Y	N	K	G	D	R	R	4
Chiken	D	-	T	F	A	E	V	R	E	D	Y	E	L	N	R	F	N	K	N	D	R	R	11
Lesser hedgehog tenrec	S	Q	S	F	T	T	N	E	E	N	Y	Q	L	L	K	F	K	L	N	D	R	R	10
Horse	S	L	T	F	E	K	S	E	E	E	H	Q	L	L	T	Y	N	K	G	D	R	R	6
Alpaca	S	L	T	F	K	E	H	E	E	D	Y	Q	L	A	I	Y	N	K	G	D	R	R	5
Bovine	S	Q	T	F	E	K	H	E	E	D	Y	Q	L	M	T	Y	N	K	G	D	R	R	3
Pig	S	L	T	F	E	K	L	E	E	D	Y	Q	L	I	T	Y	N	K	G	D	R	R	5
Goat	S	Q	T	F	E	K	H	E	E	D	Y	Q	L	M	T	Y	N	K	G	D	R	R	3
Sheep	S	Q	T	F	E	K	H	E	E	D	Y	Q	L	M	T	Y	N	K	G	D	R	R	3
Wild Bactrian camel	S	L	T	F	E	E	H	E	E	D	Y	Q	L	T	T	Y	N	K	G	D	R	R	5

Figure EV4.

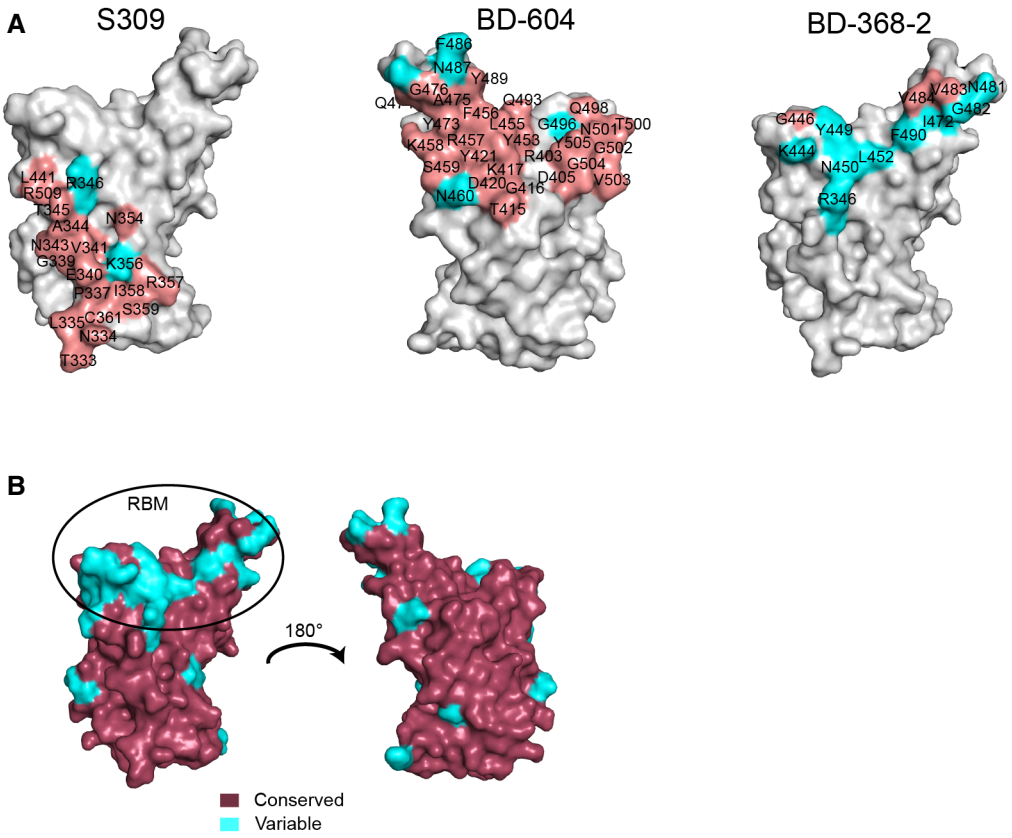

Figure EV5. Structural comparison of antibody-binding epitope and amino acid conservation in the RBD.

A Comparison of the binding interface between the SARS-CoV-2 antibody and the RshSTT182/200 RBD. In S309 (PDB: 7R6X), BD-604, and BD-368-2 (PDB: 7CHF) binding to the SARS-CoV-2 RBD site, the conserved residues between the SARS-CoV-2 and RshSTT182/200 RBDs are shown in salmon, while variable residues are shown in cyan.

B Conserved residues and variable residues between the SARS-CoV-2 and RshSTT182/200 RBDs are shown in raspberry and cyan, respectively.